

## The $B_s \rightarrow D_s^- \pi^+$ and $B_s \rightarrow D_s^\mp K^\pm$ selections

Jérémie Borel<sup>a</sup>, Louis Nicolas<sup>b</sup>,  
Olivier Schneider<sup>c</sup>, Jeroen Van Hunen<sup>d</sup>  
*Laboratoire de Physique des Hautes Energies*  
*Ecole Polytechnique Fédérale de Lausanne*

### Abstract

The decay channels  $B_s \rightarrow D_s^- \pi^+$  and  $B_s \rightarrow D_s^\mp K^\pm$  will be used to extract the physics parameters  $\Delta m_s$ ,  $\Delta \Gamma_s$  and  $\gamma + \phi_s$ . Simulation studies based on Monte Carlo samples produced in 2004 and 2005 show that a total of 140 k  $B_s \rightarrow D_s^- \pi^+$  and 6.2 k  $B_s \rightarrow D_s^\mp K^\pm$  events are expected to be triggered, reconstructed and selected in  $2 \text{ fb}^{-1}$  of data ( $10^7$  s of data taking at a luminosity of  $2 \times 10^{32} \text{ cm}^{-2} \text{ s}^{-1}$ ).

The combinatorial background-over-signal ratio originating from inclusive  $b\bar{b}$  events is expected to be  $B/S < 0.05$  at 90% CL for  $B_s \rightarrow D_s^- \pi^+$  whereas, for  $B_s \rightarrow D_s^\mp K^\pm$ , the limit is  $B/S < 0.18$  at 90% CL.

---

<sup>a</sup>jeremie.borel@epfl.ch

<sup>b</sup>louis.nicolas@epfl.ch

<sup>c</sup>olivier.schneider@epfl.ch

<sup>d</sup>jeroen.van.hunen@cern.ch

# Contents

<b>1</b>	<b>Introduction</b>	<b>2</b>
<b>2</b>	<b>Software and Monte Carlo samples</b>	<b>3</b>
<b>3</b>	<b><math>B_s \rightarrow D_s h</math> selections</b>	<b>4</b>
3.1	Generic selection without PID requirement on the bachelor . . . . .	4
3.1.1	$K$ and $\pi$ selection . . . . .	4
3.1.2	$D_s$ reconstruction . . . . .	8
3.1.3	$B_s$ reconstruction . . . . .	9
3.2	$B_s \rightarrow D_s^- \pi^+$ and $B_s \rightarrow D_s^\mp K^\pm$ selections . . . . .	9
<b>4</b>	<b>Signal yields and background levels</b>	<b>10</b>
4.1	$b$ -hadron production and branching fractions . . . . .	10
4.2	Signal efficiencies and event yields . . . . .	12
4.3	Background from minimum-bias events . . . . .	13
4.4	Background from $b\bar{b}$ events . . . . .	13
4.4.1	$b\bar{b}$ background in the $B_s \rightarrow D_s^- \pi^+$ selection . . . . .	14
4.4.2	Selected $b\bar{b}$ background in the $B_s \rightarrow D_s^\mp K^\pm$ selection . . . . .	15
4.5	Specific $B$ background contributions . . . . .	16
4.6	Summary . . . . .	16
<b>5</b>	<b>Properties of selected signal events</b>	<b>17</b>
5.1	$B_s$ mass resolution . . . . .	17
5.2	Proper-time reconstruction . . . . .	17
5.2.1	Proper-time error and pull . . . . .	18
5.2.2	Selection efficiency versus reconstructed proper-time . . . . .	18
5.2.3	Reconstruction of the $B_s$ - $\bar{B}_s$ oscillation . . . . .	19
<b>6</b>	<b>Sensitivity to <math>\Delta m_s</math></b>	<b>20</b>
<b>7</b>	<b>Conclusion</b>	<b>22</b>

# 1 Introduction

This note describes the selection of the  $B_s \rightarrow D_s^- \pi^+$  and  $B_s \rightarrow D_s^\mp K^\pm$  decays<sup>1</sup> for the LHCb experiment [1]. Although these channels are topologically very similar, the physics and hence the reasons to study them are different.

The  $B_s \rightarrow D_s^- \pi^+$  Cabibbo-favoured decay has a large branching fraction  $(3.4 \pm 0.7) \times 10^{-3}$  and can therefore be reconstructed cleanly. It is thus expected that most of the LHCb measurements of (or limits on)  $B_s$  branching fractions will be normalised to the  $B_s \rightarrow D_s^- \pi^+$  branching fraction. The  $B_s \rightarrow D_s^- \pi^+$  decay is flavour specific (i.e. the  $B_s$  flavour at decay is known from the charge of its decay products), thus this high-statistics channel is well suited for  $\Delta m_s$  measurements. It can also be used to extract information on other  $B_s - \bar{B}_s$  mixing parameters such as  $\Delta\Gamma_s$  and  $|q/p|$  (see [2] for a review on  $B_s$  oscillations). Moreover, it can be used as a control channel in time-dependent analyses of  $B_s$  decays to non flavour-specific modes, to measure the experimental dilutions due to imperfect flavour tagging.

The  $B_s \rightarrow D_s^\mp K^\pm$  Cabibbo-suppressed decays are non flavour-specific, as can be seen from the Feynman diagrams of Fig. 1. Contrary to the case where only a  $B_s$  can decay to the  $D_s^- \pi^+$  state, both a  $B_s$  and a  $\bar{B}_s$  can decay to the  $D_s^- K^+$  final state. This gives rise to the so-called mixing-induced CP violation, allowing the measurement of the weak phase  $\gamma + \phi_s$  [2].

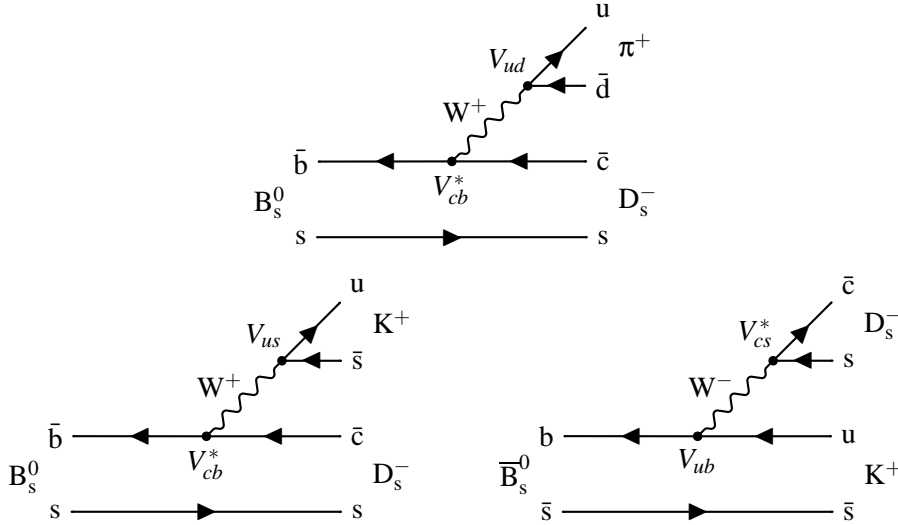


Figure 1: Feynman diagrams for the  $B_s \rightarrow D_s^- \pi^+$  and the  $B_s \rightarrow D_s^\mp K^\pm$  decays.

The  $D_s^- \pi^+$  and  $D_s^- K^+$  final states only differ by the meson produced in association with the  $D_s^-$ , which is here referred to as the *bachelor*. Hence the  $B_s \rightarrow D_s^- \pi^+$  mode will play a major role as a control channel in the analysis of  $B_s \rightarrow D_s^\mp K^\pm$  candidates. In order to reduce the systematics, it is highly desirable that the selections of  $B_s \rightarrow D_s^- \pi^+$  and  $B_s \rightarrow D_s^\mp K^\pm$  candidates be as similar as possible, sharing most of the cuts. The common part of these selections is referred to as the  $B_s \rightarrow D_s h$  selection.

In this document we consider only the  $K^- K^+ \pi^-$  final states of the  $D_s^-$  decay, including both non-resonant and resonant contributions ( $\phi\pi^-$  and  $K^{*0}K^-$ ) in an inclusive way. The mass and helicity angle cuts specific to the resonant intermediate states of the  $D_s^-$  decay

<sup>1</sup>Unless specified otherwise, charge conjugate modes are implied throughout this note.

are not used in the selection described here.

The selection relies heavily on topological cuts. Figure 2 shows the topology of a  $B_s \rightarrow D_s h$  decay. As the  $B_s$  has a lifetime of  $\sim 1.5$  ps and an average momentum of  $\sim 135$  GeV/c, it typically flies 1.1 cm before decay. This produces a displaced secondary vertex. The  $D_s$  meson has a lifetime of  $\sim 0.5$  ps and therefore produces a displaced tertiary vertex.

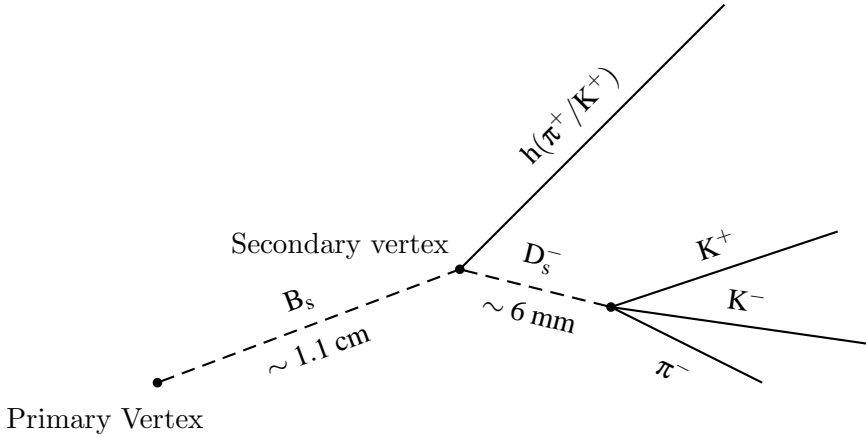


Figure 2: Topology of a  $B_s \rightarrow D_s h$  decay.

The remainder of this document is organised as follows: Section 2 describes the Monte Carlo data samples, while Section 3 gives details of the  $B_s \rightarrow D_s h$  generic selection as well as the specific cuts defining the  $B_s \rightarrow D_s^- \pi^+$  and  $B_s \rightarrow D_s^\mp K^\pm$  selections. Section 4 gives the yields and the background levels for the two selections based on explicit assumptions for the branching fractions. Finally, Section 5 outlines some properties of the selections like the mass resolution or the time distribution.

## 2 Software and Monte Carlo samples

Since the CPU resources needed to fully simulate one year of LHCb data taking are much too large, separate studies are performed using signal samples, as well as a number of background samples supposed to represent the most important contributions to the overall background.

The present study, done with LHCb analysis framework DaVinci<sup>2</sup>, is based on the data produced during the years 2004 and 2005<sup>3</sup>. Table 1 summarises the different decay channels that have been studied and the number of analysed events for each of them.

### Geometrical acceptance

In order to avoid generating unused events, a cut at 400 mrad is applied on the direction of the true signal b-hadron with respect to the beam axis. In case of inclusive  $b\bar{b}$  events, at least one b-hadron is required to pass the cut. For  $B_s$  and  $B_d$  decays, the fraction of accepted events after this geometrical cut is  $\epsilon_\theta = (35.0 \pm 0.4)\%$ . For inclusive  $b\bar{b}$  events, this factor is  $(43.4 \pm 0.3)\%$ .

<sup>2</sup>DaVinci version v12r16.

<sup>3</sup>DC04 v1, v2 and v2r3.

Decay	Number of events
$B_s \rightarrow D_s^- \pi^+$	3'990'568
$B_s \rightarrow D_s^- \mu^+ \nu X$	383'500
$B_d \rightarrow D^- \pi^+$	394'442
$B_s \rightarrow D_s^\mp K^\pm$	4'179'000
$B_s \rightarrow D_s^- \pi^+ \pi^- \pi^+$	664'500
$B_s \rightarrow D_s^- \rho^+$	529'000
$B_s \rightarrow D_s^{*-} K^+$	130'500
$B_s \rightarrow D_s^{*-} \pi^+$	157'500
inclusive $b\bar{b}$	27'291'931
minimum bias	48'254'400

Table 1: MC samples used in this study. In all  $B_s$  samples the  $D_s^-$  meson was forced to decay to the  $K^- K^+ \pi^-$  final state including both resonant ( $\phi\pi^-$ ,  $K^{*0}K^-$ ) and non-resonant modes. In the  $B_d \rightarrow D^- \pi^+$  sample, the decay  $D^- \rightarrow K^- \pi^- \pi^+$  was forced. See [3] for a complete definition of the decay modes.

### 3 $B_s \rightarrow D_s h$ selections

This study super-seeds (but is inspired from) the  $B_s \rightarrow D_s h$  selection developed in [4]. The selection performance is estimated using data samples different from those used to define most of the selection cuts. Only the particle identification (PID) cuts have been tuned on the same samples as those used to quantify the selection efficiency.

#### 3.1 Generic selection without PID requirement on the bachelor

The cuts of this selection have been chosen using the following method: for each selection variable, the distribution of Monte Carlo  $B_s \rightarrow D_s h$  signal events is studied. A loose pre-selection is then defined with the aim to remove as little signal as possible. This pre-selection, which rejects the large part of the combinatorial background, is applied on signal and inclusive  $b\bar{b}$  events. At this point, the comparison of pre-selected signal and background distributions allows to choose selection cuts that maintain a reasonable signal efficiency while reducing drastically the  $b\bar{b}$  background. The choice of cut values does not follow a well defined optimisation procedure. This will be done once one knows better the real background in the data.

The distributions of the different selection variables are shown in Figs. 3, 4 and 5, after all pre-selection cuts. Their area is normalised to one.

##### 3.1.1 K and $\pi$ selection

Every reconstructed long track<sup>4</sup> has to fulfil the following kinematic requirements: its momentum ( $p$ ) has to be larger than 2 GeV (Fig. 3(a)) and its transverse momentum<sup>5</sup> ( $p_T$ )

<sup>4</sup>Long tracks are reconstructed tracks that leave at least 3  $r$  and 3  $\phi$  associated clusters in the VeLo and at least 1  $x$  and 1 stereo hit in each the tracking stations (T1-T3).

<sup>5</sup> $p_T$  is computed with respect to the  $z$ -axis ( $p_T \equiv \sqrt{p_x^2 + p_y^2}$ ) and not to the B-meson direction. This approximation is possible because the B meson tends to fly along the  $z$ -axis.

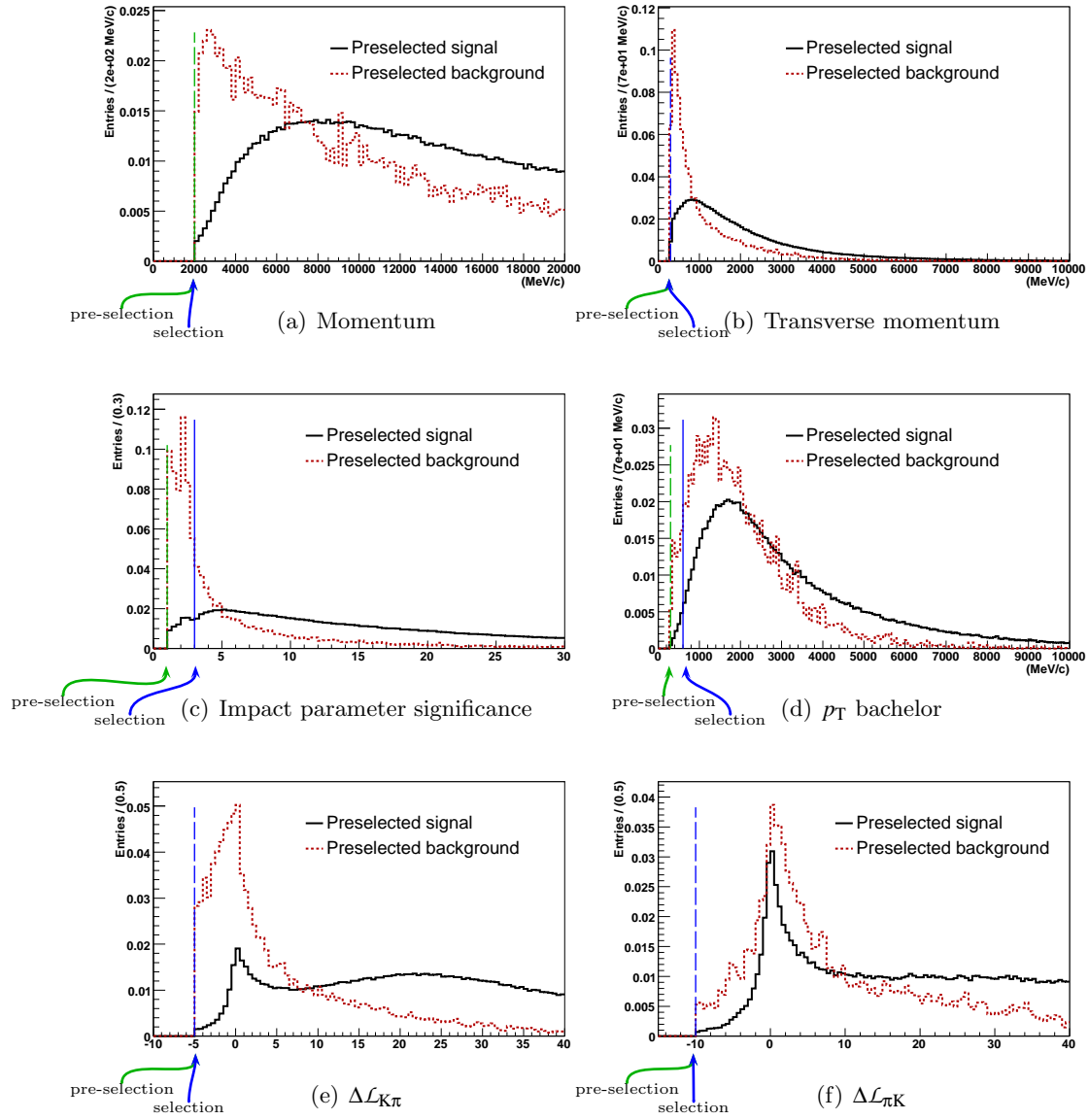


Figure 3: Distributions of the different variables for all the particles from the decay (pions and kaons). The pre-selection and selection cuts are indicated.

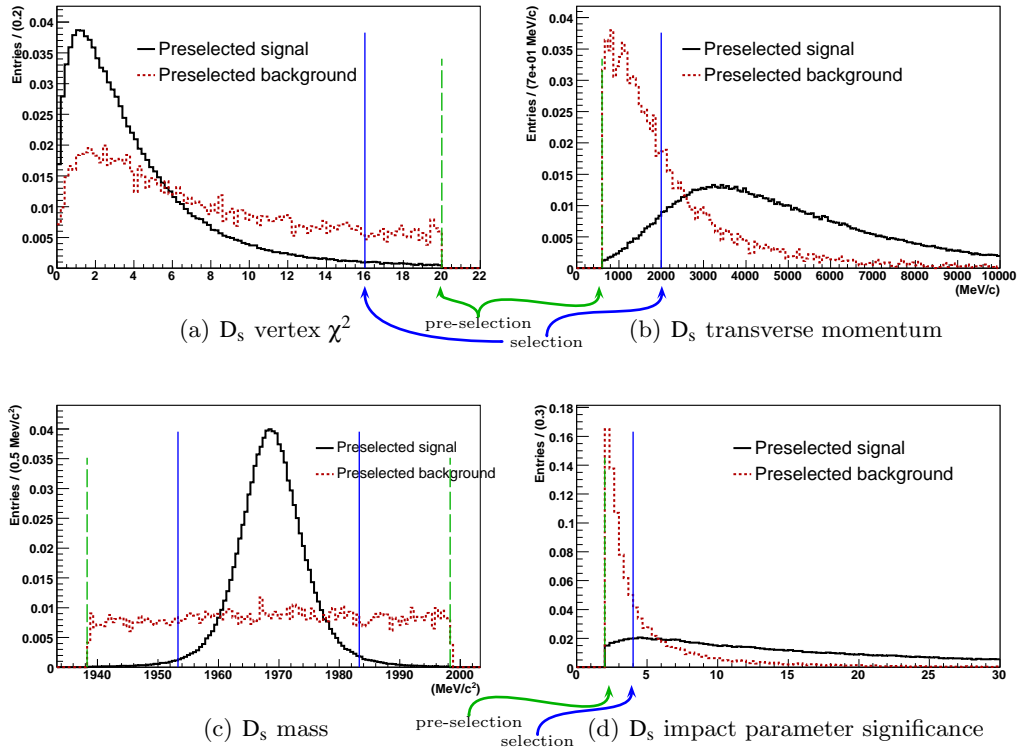


Figure 4:  $D_s$  selection variable. The pre-selection and selection cuts are indicated.

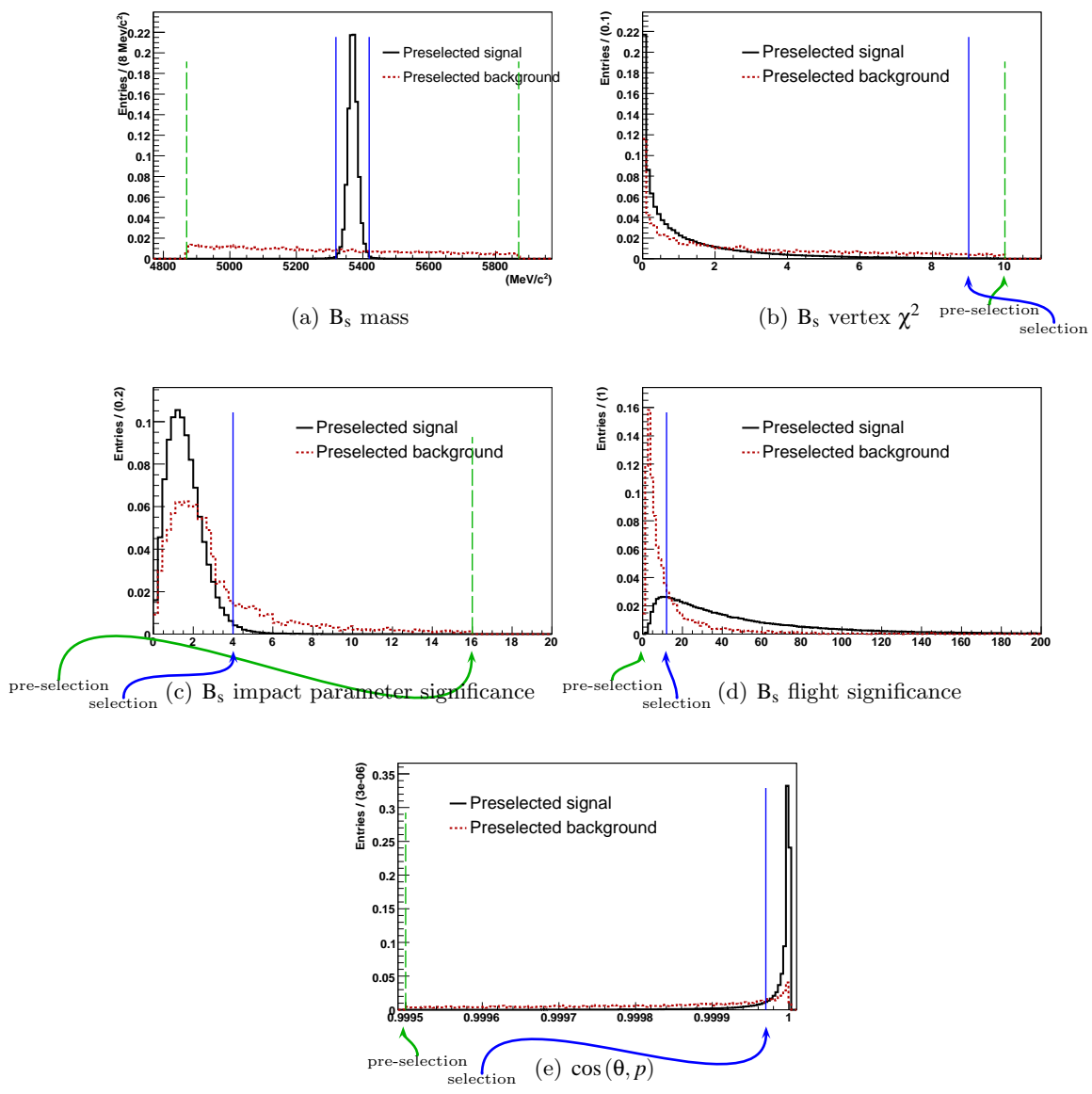


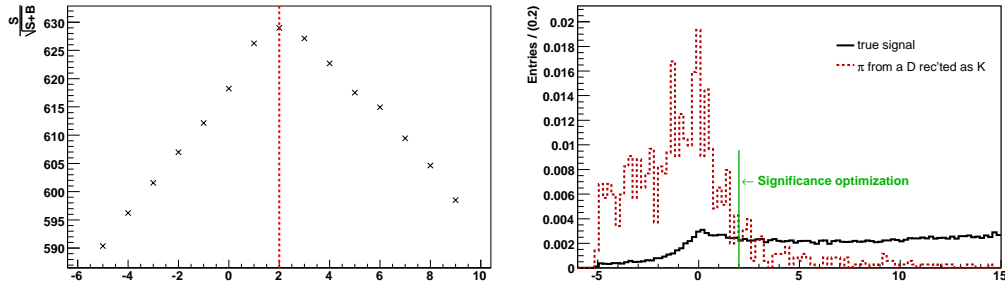
Figure 5:  $B_s$  selection variables. The pre-selection and selection cuts are indicated.



should be larger than 300 MeV (Fig. 3(b)). An impact parameter significance<sup>6</sup> (IPS) bigger than three with respect to each primary vertex is also required (Fig. 3(c)) (At the luminosity of  $2 \times 10^{-32} \text{ cm}^{-2}\text{s}^{-1}$  about 35% of the events have two more than one primary vertexes). The track will be used as a kaon if it satisfies a Delta Log Likelihood<sup>7</sup> of  $\Delta\mathcal{L}_{K\pi} > -5$  and  $\Delta\mathcal{L}_{Kp} > -10$  (Fig. 3(e)), and it will be used as a pion if  $\Delta\mathcal{L}_{\pi K} > -10$  (Fig. 3(f)). Hence, a track can be tagged simultaneously as both  $\pi$  and K.

### 3.1.2 $D_s$ reconstruction

To reconstruct  $D_s^- \rightarrow K^+K^-\pi^-$  candidates, every combination of  $K^+K^-\pi^-$  tracks is tested. To reject the specific background coming from  $B_d \rightarrow D^-\pi^+$  and  $B_d \rightarrow D^-K^+$ , where the  $D^-$  decays to  $K^-\pi^+\pi^-$  (whereas the  $D_s^-$  decays to  $K^-K^+\pi^-$ ) it is required that  $\Delta\mathcal{L}_{K\pi} > 2$  on the  $D_s$  daughters reconstructed as kaon. The value of this cut has been tuned on  $B_s \rightarrow D_s^-\pi^+$  signal sample with  $B_d \rightarrow D^-\pi^+$  decays as background. The significance value ( $S/\sqrt{S+B}$ ) versus the PID cut is shown in Fig. 6(a), and the PID spectrum for signal and background can be seen in Fig 6(b). As the situation also applies to the  $B_s \rightarrow D_s^\mp K^\pm$  selection with the  $B_d \rightarrow D^-K^+$  background and because they have the same relative branching fraction (i.e  $\mathcal{B}(B_d \rightarrow D^-\pi^+) \simeq \mathcal{B}(B_s \rightarrow D_s^-\pi^+)$  and  $\mathcal{B}(B_d \rightarrow D^-K^+) = \mathcal{B}(B_s \rightarrow D_s^\mp K^\pm)$ ) we apply this cut in the  $B_s \rightarrow D_s h$  selection and not in the  $B_s \rightarrow D_s^-\pi^+$  specific selection.



(a) Signal significance versus  $\Delta\mathcal{L}_{K\pi}$ .

(b)  $\Delta\mathcal{L}_{K\pi}$  from the  $D_s$  daughters reconstructed as kaons for 1)  $B_s \rightarrow D_s^-\pi^+$  events (continuous line) and 2)  $B_d \rightarrow D^-\pi^+$  events reconstructed as  $B_s \rightarrow D_s^-\pi^+$  (dashed red line). The histogram overflows are not plotted

Figure 6: PID cut on the  $D_s$  daughters with  $B_s \rightarrow D_s^-\pi^+$  as signal.

Moreover, only  $D_s$  candidates with a vertex fit  $\chi^2$  lower than 16 are kept (Fig. 4(a)), they must also have a transverse momentum larger than 2 GeV (Fig. 4(b)) and should have an invariant mass within 15 MeV of the  $D_s$  mass (Fig. 4(c)). Finally, to ensure a well displaced secondary vertex, a four sigma significance is required on the  $D_s$  impact parameter (Fig. 4(d)) with respect to each primary vertex.

<sup>6</sup>The Impact Parameter Significance is defined as the track impact parameter with respect to a primary vertex divided by its error:  $IPS \equiv \left(\frac{IP}{\sigma_{IP}}\right)$ .

<sup>7</sup>For a given reconstructed particle  $p$ ,  $\Delta\mathcal{L}_{p_1 p_2}$  is a quantity quantifying the hypothesis that this particle is of type  $p_1$  rather than  $p_2$ .

### 3.1.3 $B_s$ reconstruction

A  $B_s$  is reconstructed out of a  $D_s$  and a bachelor track. The following conditions must be fulfilled by each candidate: the reconstructed invariant mass should be within a  $\pm 50$  MeV window around the  $B_s$  mass (Fig. 5(a)). The  $\chi^2$  of the  $B_s$  decay vertex must be smaller than 9 (Fig. 5(b)). To ensure that the reconstructed  $B_s$  does come from a primary vertex, the smallest impact parameter significance with respect to each primary vertex has to be smaller than 4 (Fig. 5(c)). The flight distance significance from this primary vertex must be larger than 12 (Fig. 5(d)) and the cosine of the  $B_s$  pointing angle has to be larger than 0.99997 (Fig. 5(e)). Pointing angle here means the angle between the particle's reconstructed momentum and its flight direction, defined by the  $B_s$  decay vertex and its associated primary vertex. Table 2 summarises the cut values.

Cuts on all the kaons and pions	Pre-selection	Selection
for pions : $\Delta\mathcal{L}_{\pi K}$	> -10	> -10
for kaons : $\Delta\mathcal{L}_{Kp}$	> -10	> -10
IPS	> 1	> 3
Cuts on the bachelor	Pre-selection	Selection
$p_h$ (MeV)	> 2000	> 2000
$p_{T,h}$ (MeV)	> 300	> 600
for kaons : $\Delta\mathcal{L}_{K\pi}$	> -5	> -5*
Cuts on the $D_s$ and its daughters	Pre-selection	Selection
$p_{D_s}$ on the $D_s$ daughters (MeV)	> 2000	> 2000
$p_T$ for the $D_s$ daughters (MeV)	> 300	> 300
for kaons : $\Delta\mathcal{L}_{K\pi}$	> -10	> 2
$p_{T,D_s}$ (MeV)	> 500	> 2000
IPS $_{D_s}$	> 2	> 4
$D_s$ vertex $\chi^2$	< 20	< 16
$\Delta M_{D_s}$ (MeV)	$\pm$ 30	$\pm$ 15
Cuts on the $B_s$	Pre-selection	Selection
IPS $_{B_s}$	< 16	< 4
$B_s$ vertex $\chi^2$	< 10	< 9
$\Delta M_{B_s}$ (MeV)	$\pm$ 500	$\pm$ 50
FS $_{B_s-PV}$	> 0	> 12
$z_{D_s} - z_{B_s}$ (mm)	> 0	> 12
$\cos\theta_p$	> 0.9995	> 0.99997

\* This cut change in the specific  $B_s \rightarrow D_s^\mp K^\pm$  selection, see Section 3.2.

Table 2: Cut values for the  $B_s \rightarrow D_s h$  pre-selection and selection.

### 3.2 $B_s \rightarrow D_s^- \pi^+$ and $B_s \rightarrow D_s^\mp K^\pm$ selections

These two selections are derived from the generic  $B_s \rightarrow D_s h$  selection. For  $B_s \rightarrow D_s^- \pi^+$  events, we simply require that the bachelor is identified as a pion. For  $B_s \rightarrow D_s^\mp K^\pm$ , an additional PID cut on the bachelor is needed to get rid of the  $B_s \rightarrow D_s^- \pi^+$  background.

Other background contributions like  $B_s \rightarrow D_s^- \ell^+ \nu X$  happened to be too marginal in the  $B_s \rightarrow D_s h$  selection to justify a specific cut.

For the  $B_s \rightarrow D_s^\mp K^\pm$  selection, one has to cope with the  $B_s \rightarrow D_s^- \pi^+$  background. Thus we add a PID cut on the bachelor of reconstructed  $B_s \rightarrow D_s h$  events (see Fig. 7). The cut value has been chosen by optimising the significance  $\frac{S}{\sqrt{S+B}}$ , where  $S$  and  $B$  are the signal and background yields respectively. Since the uncertainty of the branching fractions which are involved are large (see Section 4.1), the systematic errors on the significance are rather big.

The significance plot 7(a) shows a plateau starting at 4, we use this value for the  $\Delta\mathcal{L}_{K\pi}$  cut on the bachelor for the  $B_s \rightarrow D_s^\mp K^\pm$  offline selection. This PID cut implies a signal yield reduction of about 17%. On the other hand, the yield of  $B_s \rightarrow D_s^- \pi^+$  events reconstructed as  $B_s \rightarrow D_s^\mp K^\pm$  is reduced by 95%.

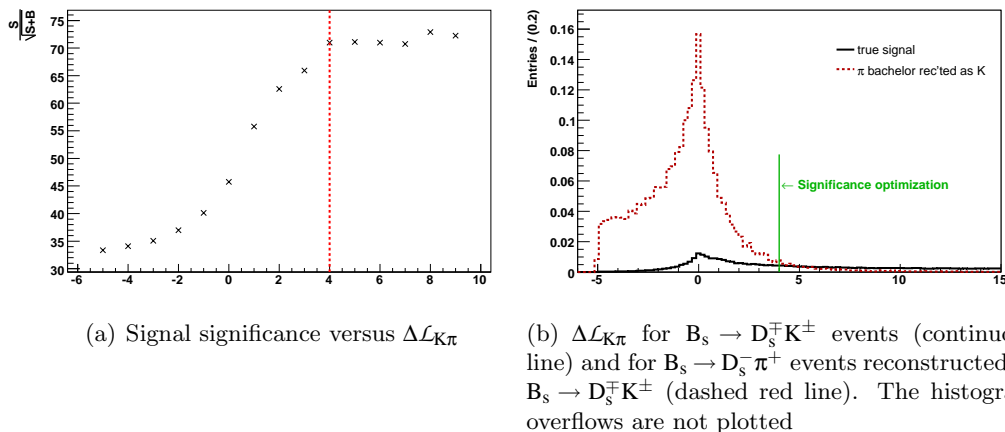


Figure 7: PID cut on the bachelor with  $B_s \rightarrow D_s^\mp K^\pm$  as signal.

## 4 Signal yields and background levels

Since the yield estimates rely on the b-hadron production cross section and on branching fractions, this section begins with a description of the values which have been used for this calculation.

### 4.1 b-hadron production and branching fractions

Table 3 shows the different branching fractions used for the present selection. Most values come from the PDG [5]. In particular, the  $D_s^+ \rightarrow \phi \pi^+$  branching fraction is taken from the PDG although its value is subject to discussion [6]. The branching fractions for  $B_s \rightarrow D_s^- \pi^+$  and  $B_s \rightarrow D_s^- \ell^+ \nu X$  do not come from the PDG and are explained below:

$\mathcal{B}(B_s \rightarrow D_s^- \pi^+)$ : In previous studies [1] the  $B_s \rightarrow D_s^- \pi^+$  branching fraction was assumed to be equal to the one of  $B_d \rightarrow D^- \pi^+$ . However, two measurements of the  $B_s \rightarrow D_s^- \pi^+$  branching fraction have recently been performed.

The CDF collaboration has measured the following ratio [7]:

$$\begin{aligned} \frac{\mathcal{B}(\mathbf{B}_s \rightarrow \mathbf{D}_s^- \pi^+)}{\mathcal{B}(\mathbf{B}_d \rightarrow \mathbf{D}^- \pi^+)} &= \frac{N(\mathbf{B}_s) \varepsilon(\mathbf{B}_d) f_{\mathbf{B}_d}}{N(\mathbf{B}) \varepsilon(\mathbf{B}_s) f_{\mathbf{B}_s}} \times \frac{\mathcal{B}(\mathbf{D}^- \rightarrow \mathbf{K}^+ \pi^- \pi^-)}{\mathcal{B}(\mathbf{D}_s^- \rightarrow \phi \pi^-) \mathcal{B}(\phi \rightarrow \mathbf{K}^- \mathbf{K}^+)} \\ &= 1.13 \pm 0.08(\text{stat.}) \pm 0.05(\text{syst.}) \pm 0.15(\text{BF}) \pm 0.17(\text{PF}) \end{aligned} \quad (1)$$

where the two last errors come from the  $\mathbf{D}$ ,  $\mathbf{D}_s$  and  $\phi$  branching fractions and the hadronization fractions respectively.  $f_{\mathbf{B}_s}$  stands for the  $\mathbf{B}_s$  production fraction and  $\varepsilon(\mathbf{B}_s)$  for the CDF's detection efficiency of these mesons. Multiplying this value by  $\mathcal{B}(\mathbf{D}_s^- \rightarrow \phi \pi^-) = (4.4 \pm 0.6)\%$  [5] and  $\mathcal{B}(\mathbf{B}_d \rightarrow \mathbf{D}^- \pi^+) = (2.83 \pm 0.17) \times 10^{-3}$  [5] and combining all the errors quadratically, we get:

$$\mathcal{B}(\mathbf{B}_s \rightarrow \mathbf{D}_s^- \pi^+)_{\text{CDF}} \times \mathcal{B}(\mathbf{D}_s^- \rightarrow \phi \pi^-) = (1.4 \pm 0.3) \times 10^{-4}. \quad (2)$$

The second measurement comes from the Belle collaboration [8]:

$$\mathcal{B}(\mathbf{B}_s \rightarrow \mathbf{D}_s^- \pi^+)_{\text{Belle}} = (0.68 \pm 0.22 \pm 0.16)\%. \quad (3)$$

It is based on three different  $\mathbf{D}_s^-$  decay modes, namely  $\phi \pi^-$ ,  $\mathbf{K}^* \mathbf{K}^-$  and  $\mathbf{K}_S^0 \mathbf{K}^-$ . Assuming that the reconstruction efficiency is similar for these three modes and knowing that the  $\mathbf{D}_s^- \rightarrow \mathbf{K}^* \mathbf{K}^-$  and  $\mathbf{D}_s^- \rightarrow \mathbf{K}_S^0 \mathbf{K}^-$  have been measured relative to the  $\mathbf{D}_s^- \rightarrow \phi \pi^-$  branching fraction, we compute:

$$\mathcal{B}(\mathbf{B}_s \rightarrow \mathbf{D}_s^- \pi^+)_{\text{Belle}} \times \mathcal{B}(\mathbf{D}_s^- \rightarrow \phi \pi^-) = (3.0 \pm 1.1) \times 10^{-4}. \quad (4)$$

The two values given in (2) and (4) are independent because the correlation between the original measurements (1) and (3) has been removed. They are compatible within 1.14 sigma. Their weighted average divided by  $\mathcal{B}(\mathbf{D}_s^- \rightarrow \phi \pi^-) = (4.4 \pm 0.6)\%$  [5], leads to:

$$\mathcal{B}(\mathbf{B}_s \rightarrow \mathbf{D}_s^- \pi^+) = (3.4 \pm 0.7) \times 10^{-3}.$$

The latter value is the one used in this document.

It is also possible to compute two independent values of  $\frac{\mathcal{B}(\mathbf{B}_s \rightarrow \mathbf{D}_s^- \pi^+)}{\mathcal{B}(\mathbf{B}_d \rightarrow \mathbf{D}^- \pi^+)} \times \mathcal{B}(\mathbf{D}_s^- \rightarrow \phi \pi^-)$ , one from Belle and one from CDF. Then one can average them and divide by  $\mathcal{B}(\mathbf{D}_s^- \rightarrow \phi \pi^-)$ . The result

$$\frac{\mathcal{B}(\mathbf{B}_s \rightarrow \mathbf{D}_s^- \pi^+)}{\mathcal{B}(\mathbf{B}_d \rightarrow \mathbf{D}^- \pi^+)} = 1.18 \pm 0.25$$

shows that the assumption  $\mathcal{B}(\mathbf{B}_s \rightarrow \mathbf{D}_s^- \pi^+) = \mathcal{B}(\mathbf{B}_d \rightarrow \mathbf{D}^- \pi^+)$  is still compatible with the available experimental results.

**$\mathbf{B}_s \rightarrow \mathbf{D}_s^- \ell^+ \nu \mathbf{X}$ :** The PDG value uses three measurements [9, 10, 11]. However, the average value is still based on an old value of the  $\mathbf{D}_s^- \rightarrow \phi \pi^-$  branching fraction. We updated this value and obtained a weighted mean of  $\text{BR}(\mathbf{B}_s \rightarrow \mathbf{D}_s^- \ell^+ \nu \mathbf{X}) = (6.7 \pm 1.6)\%$ . Concerning this decay, we do the assumption that we can estimate its reconstruction efficiency from a sample of  $\mathbf{B}_s \rightarrow \mathbf{D}_s^- \mu^+ \nu \mathbf{X}$  decay.

Decay	value	estimated as	Ref.
$B_s \rightarrow D_s^- \pi^+$	$(3.4 \pm 0.7) \times 10^{-3}$	see 4.1	[7, 8, 5]
$B_s \rightarrow D_s^- \ell^+ \nu X$	$(6.7 \pm 1.6) \times 10^{-2}$	see 4.1	[9, 10, 11, 5]
$B_s \rightarrow D_s^{*-} \pi^+$	$(2.76 \pm 0.21) \times 10^{-3}$	$B_d \rightarrow D^{*-} \pi^+$	[5]
$B_s \rightarrow D_s^- \rho^+$	$(7.5 \pm 1.2) \times 10^{-3}$	$B_d \rightarrow D^- \rho^+$	[5]
$B_s \rightarrow D_s^- K^+$	$(2.0 \pm 0.6) \times 10^{-4}$	$B_d \rightarrow D^- K^+$	[5]
$B_s \rightarrow D_s^+ K^-$	$(2.2 \pm 0.7) \times 10^{-5}$	$B_d \rightarrow D_s^+ \pi^-$	[5]
$B_s \rightarrow D_s^{\mp} K^{\pm}$	$(2.2 \pm 0.6) \times 10^{-4}$	sum of above two	
$B_s \rightarrow D_s^{*-} K^+$	$(2.14 \pm 0.20) \times 10^{-4}$	$B_d \rightarrow D^{*-} K^+$	[5]
$B_s \rightarrow D_s^- \pi^+ \pi^- \pi^+$	$(8.0 \pm 2.5) \times 10^{-3}$	$B_d \rightarrow D^- \pi^+ \pi^+ \pi^-$	[5]
$B_d \rightarrow D^- \pi^+$	$(2.83 \pm 0.17) \times 10^{-3}$		[5]
$D_s^+ \rightarrow K^+ K^- \pi^+$	$(5.2 \pm 0.9) \times 10^{-2}$		[5]
$D^+ \rightarrow K^- \pi^+ \pi^+$	$(9.51 \pm 0.34) \times 10^{-2}$		[5]
$f_{B_s}$	$(10.3 \pm 1.3) \times 10^{-2}$		[5]
$f_{B_d}$	$(39.8 \pm 1.2) \times 10^{-2}$		[5]

Table 3: Branching fraction values assumed in the calculation of the yields and background levels.  $f_{B_s}$  and  $f_{B_d}$  refer to the  $B_s$  and  $B_d$  production fractions respectively.

## 4.2 Signal efficiencies and event yields

Table 4 shows the efficiencies computed for  $B_s \rightarrow D_s^- \pi^+$  and  $B_s \rightarrow D_s^{\mp} K^{\pm}$  decays. As a reminder, the values for the total efficiencies  $\epsilon_{\text{tot}}$  published in [1] were 0.337% and 0.269% for  $B_s \rightarrow D_s^- \pi^+$  and  $B_s \rightarrow D_s^{\mp} K^{\pm}$  respectively. One difference is that the Technical Design Review (TDR) did not take any High Level Trigger (HLT) into account whereas the new values are computed out of events that pass this trigger<sup>8</sup>. A breakdown of the efficiency is given, the description of this breakdown can be found in [1]. The total efficiency, in the last column of Table 4, is the product of all the other efficiencies.

This study	$\epsilon_{\text{det}}[\%]$	$\epsilon_{\text{rec/det}}[\%]$	$\epsilon_{\text{sel/rec}}[\%]$	$\epsilon_{\text{trg/sel}}[\%]$	$\epsilon_{\text{tot}}[\%]$
$B_s \rightarrow D_s^- \pi^+$	6.3	78.4	25.7	30	0.39
$B_s \rightarrow D_s^{\mp} K^{\pm}$	6.1	80.4	22.4	29	0.32

Table 4: Efficiencies for  $B_s \rightarrow D_s^- \pi^+$  and  $B_s \rightarrow D_s^{\mp} K^{\pm}$ . The errors from the Monte Carlo statistics are of the order of the first unprinted digit.

## Yield computation

The yield for a decay channel  $i$  is computed as

$$Y_i = L_{\text{int}} \times \sigma_{b\bar{b}} \times 2 \times f_{B_i} \times \text{BR}_i^{\text{vis}} \times \epsilon_{\text{tot},i},$$

where  $L_{\text{int}} = 2 \text{ fb}^{-1}$  is the integrated luminosity after  $10^7$  seconds of data taking at an average instantaneous luminosity of  $2 \times 10^{32} \text{ cm}^{-2} \text{ s}^{-1}$ , and  $\sigma_{b\bar{b}} = 500 \mu\text{b}$  is the expected  $b\bar{b}$  production cross-section. The factor 2 stands for the two  $b$  quarks and  $f_{B_i}$  is the probability for a  $b$ -quark to hadronize in the involved B meson.  $\text{BR}_i^{\text{vis}}$  is the total visible

<sup>8</sup>The HLT version applied is v4r1

branching fraction –defined as the product of all the different branching fractions involved in the decay chain– of the decay channel  $i$ .  $\epsilon_{\text{tot},i}$  is the total trigger and selection efficiency (i.e. the number of triggered and selected events divided by the number of events processed times the geometrical acceptance  $\epsilon_{\theta}$  as defined in Section 2).

The yields shown in Table 5 correspond to events that pass the HLT trigger and assuming a statistics of  $2 \text{ fb}^{-1}$  of data.

### Signal yields

$B_s \rightarrow D_s^- \pi^+$	140 k $\pm$	0.67 k (stat.) $\pm$	40 k (syst.)
$B_s \rightarrow D_s^{\mp} K^{\pm}$	6.2 k $\pm$	0.03 k (stat.) $\pm$	2.4 k (syst.)

Table 5: Expected signal yields after trigger in  $2 \text{ fb}^{-1}$  of data. The quoted systematic uncertainties come from  $f_{B_s}$  and the branching fraction uncertainties given in table 3. The uncertainty on  $\sigma_{b\bar{b}}$  is not included.

### 4.3 Background from minimum-bias events

A *minimum-bias* sample contains at generator level all kinds of events that can occur in a  $pp$ -collision in natural proportions.

The  $B_s \rightarrow D_s h$  offline selection has been tested on 131 k minimum-bias events passing the L0 and L1 triggers<sup>9</sup>. This represents 48 M events before trigger and about 3 s of LHCb running at a luminosity of  $2 \times 10^{-32} \text{ cm}^{-2} \text{ s}^{-1}$ . No event passes the selection. However, due to the large minimum-bias cross section (103.4 mb in the Monte Carlo) one cannot retrieve a meaningful limit to the background from this analysis.

### 4.4 Background from $b\bar{b}$ events

Events containing a  $b\bar{b}$  quark pair represent the main source of background since they have a displaced vertex and are thus easily accepted by the triggers. A total of 27.3 M of  $b\bar{b}$  events were analysed, corresponding to 117 seconds at the nominal luminosity of  $2 \times 10^{32} \text{ cm}^{-2} \text{ s}^{-1}$ . To cope with the fact that very few  $b\bar{b}$  events pass the selection, we artificially increase the statistics by enlarging the  $B_s$  mass window to  $\pm 500 \text{ MeV}$  (whereas the nominal cut is  $\pm 50 \text{ MeV}$ ). Moreover, no trigger decision is required during the selection. We assume that this is conservative for the computation of the  $B/S$  ratio.

In this sample, three  $B_s \rightarrow D_s^- \pi^+$  decays were correctly identified from the  $b\bar{b}$  sample. Given the branching fractions used for the generation and the total signal efficiency determined on a large signal sample, 1.5 event was expected. No  $B_s \rightarrow D_s^{\mp} K^{\pm}$  event was selected, which is consistent with the 0.1 event expected. This data sample has also been used to identify some potentially dangerous specific background. Dedicated studies have been done on these event types, namely on  $B_d \rightarrow D^- \pi^+$ ,  $B_s \rightarrow D_s^{*-} \pi^+$ ,  $B_s \rightarrow D_s^{*-} K^+$ ,  $B_s \rightarrow D_s^- \rho^+$ ,  $B_s \rightarrow D_s^- \mu^+ \nu X$  and  $B_s \rightarrow D_s^- \pi^+ \pi^- \pi^+$ .

<sup>9</sup>Until mid 2006, the LHCb design was made of three trigger levels: L0, L1 and HLT. However, in the current design, the L1 trigger has been merged with the HLT. For clarity, the rest of this document will refer to the HLT as a merged version of the L1 and the ‘old’ HLT. The triggers were those defined in DaVinci v12r15: L0 v6r7p7 and L1 v4r7.

#### 4.4.1 $b\bar{b}$ background in the $B_s \rightarrow D_s^- \pi^+$ selection

A particle can be reconstructed or associated in different ways, leading to more than one candidate per event. In addition to that, some events have sometimes more than one collision which can also give multiple candidates for one event. This is why the following list describes the candidates that are reconstructed and not the events.

In the inclusive  $b\bar{b}$  sample, 56 candidates are reconstructed as  $B_s \rightarrow D_s^- \pi^+$  and pass the loose mass window. These candidates are described below using the information from the Monte Carlo truth:

- 36 events do not pass the tight mass window. As they are reconstructed from a peaking background, they should not be counted in the statistics. However, some of them can potentially fall in the tight  $B_s$  mass window. The list below describes from which Monte Carlo particles they were reconstructed and the reasons why they are not counted into the  $B/S$  background. Some of the channels have required a dedicated study. Their results are shown in Section 4.5.

13 events come from a  $B_s \rightarrow D_s^{*-} \pi^+$  decay. This channel has been studied on a dedicated sample. Its  $B/S$  contribution is lower than  $4 \times 10^{-3}$  at 90% CL.

15 are reconstructed from a  $B_s \rightarrow D_s^{(*)-} \rho^+$  decay. The  $B_s \rightarrow D_s^- \rho^+$  channel has been studied separately, its  $B/S$  value is lower than  $2 \times 10^{-3}$  at 90% CL.

1 event is a  $B_s \rightarrow D_s^- \mu^+ \nu$  decay. Again, a dedicated study shows a  $B/S$  upper limit of  $2 \times 10^{-2}$  at 90% CL.

1 event is a  $B_d \rightarrow D_s^- \pi^+$  decay. It does not pass the tight  $B_s$  mass requirement. Though it is not possible to ignore this channel *a priori*, we assume it has the same reconstruction efficiency as  $B_s \rightarrow D_s^- \pi^+$  events except for the  $B_s$  mass window cut. Assuming a Gaussian mass distribution with the same sigma (14 MeV) as the signal mass spectrum, we see that only 0.3% of the reconstructed  $B_d \rightarrow D_s^- \pi^+$  decays will pass the tight  $B_s$  mass window. The  $B_d \rightarrow D_s^- \pi^+$  branching fraction, according to [5] is 200 times lower than the  $B_s \rightarrow D_s^- \pi^+$  branching fraction. This allows to compute a limit to the  $B/S$  contribution of  $4 \times 10^{-6}$ .

2 events come from  $B_d \rightarrow D_s^{*-} \pi^+$  decays. The upper limit to the branching fraction according to [5] is 67 times lower than the  $B_s \rightarrow D_s^{*-} \pi^+$  value. The reconstruction efficiency cannot be higher than  $B_s \rightarrow D_s^{*-} \pi^+$ . This gives a  $B/S$  upper limit of  $3 \times 10^{-6}$ .

1 event comes from a  $B_d \rightarrow D_s^- \rho^+$  decay. Its branching fraction is lower than  $6 \times 10^{-4}$  at 90% CL [5]. Its reconstruction efficiency cannot be bigger than the  $B_s \rightarrow D_s^- \rho^+$  channel. Thus  $1 \times 10^{-5}$  is an upper limit for this background.

2 events are  $B_d \rightarrow D_s^{*-} \ell^+ \nu_\ell$  decays. There is no branching fraction estimate for this channel. However, the mother particle is a  $B_d$  and not a  $B_s$ , the neutrino as well as the  $\pi^0$  or the  $\gamma$  arising from the  $D_s^*$  are not reconstructed. This results in a lower reconstructed  $B_s$  mass.

1 event comes from a  $B^+ \rightarrow D_s^+ \rho^0$  decay. It is low mass background since the mass difference between the  $B^+$  and the  $B_s$  plus the pion mass from the  $\rho^0$  which is not reconstructed, give a 230 MeV shift to the reconstructed  $B_s$  mass.

- 1 event is reconstructed from a  $B_d \rightarrow D^- K^+$  decay where a double pion/kaon mis-identification allows the reconstruction of a  $B_s \rightarrow D_s^- \pi^+$  event. Here, two effects

partially cancel: the  $B_d$  mass is lower than the  $B_s$  mass, but the double pion/kaon mis-identification tends to shift the mass to higher value. Although this event does not pass the tight mass requirement, it cannot be neglected and has been included in the  $B/S$  estimation.

- 2 events contain a  $B_d \rightarrow D^- \pi^+$  decays. Here again, a mis-identification in the  $D^-$  daughters allows the reconstruction of a  $D_s^-$ . The two events pass the tight mass window requirement and are counted in the  $B/S$  estimation.
- 9 events come from a mis-reconstructed  $\Lambda_b$  decay. Though its mass (5624 MeV) is much larger than the 5419.6 MeV upper value of the  $B_s$  mass window (the difference is  $\sim 14$  times the  $B_s$  mass resolution), the mis-identification of a true proton as a pion brings the reconstructed  $B_s$  mass in the tight mass requirement. Three different decay channels are present:  $\Lambda_b \rightarrow D_s^- p$  and  $\Lambda_b \rightarrow \Lambda_c^- \pi^+$  which imply a single pion/proton mis-identification, and  $\Lambda_b \rightarrow D_s^{*-} p$  which, beside the  $\pi/p$  mis-identification, also imply the loss of a photon. These events tend to be in the tight mass window. They could be rejected with a  $\Delta\mathcal{L}_{\pi p}$  cut though this has not been studied. Three out of these nine fall into the tight mass window. They have been included in the estimation of the  $b\bar{b}$  background.
- The 8 remaining events are either ghosts (3), or pure combinatorial (5).

Thus 8 combinatorial (downscaled by the mass ratio) and  $3(\Lambda_b \text{ events}) + 2(B_d \rightarrow D^- \pi^+) + 1(B_d \rightarrow D^- K^+) = 6$  specific events (which are not downscaled by the mass ratio) remain for the  $B/S$  computation. Separated limits are given. For the combinatorial background contribution, the central value is  $0.027 \pm 0.008$  and the 90% CL interval according to [12] is:

$$\frac{B^{\text{combinatorial}}}{S_{(B_s \rightarrow D_s^- \pi^+)}} \in [0.014, 0.05] \text{ at 90\% CL,}$$

whereas for the specific contribution, the central value is  $0.21 \pm 0.06$  and the confidence interval is:

$$\frac{B^{\text{specific}}}{S_{(B_s \rightarrow D_s^- \pi^+)}} \in [0.08, 0.4] \text{ at 90\% CL.}$$

#### 4.4.2 Selected $b\bar{b}$ background in the $B_s \rightarrow D_s^\mp K^\pm$ selection

The  $B_s \rightarrow D_s^\mp K^\pm$  selection keeps 3 candidates in the loose mass window. From the MC information of these events, one can see the following:

- Two events contain  $B_d \rightarrow D_s^- K^+$  decays. They do not pass the tight  $B_s$  mass requirement. Using the same argument as for the  $B_d \rightarrow D_s^- \pi^+$  decay above, 0.3% of the events will fall into the tight  $B_s$  mass window. The PDG gives a 90% CL upper limit to the  $B_d \rightarrow D_s^- K^+$  branching fraction of  $2.5 \times 10^{-5}$ , which is 9 times less than the  $B_s \rightarrow D_s^\mp K^\pm$  branching fraction. This allows to compute an upper limit to the  $B/S$  contribution –assuming a reconstruction efficiency of 0.3% times the  $B_s \rightarrow D_s^\mp K^\pm$  reconstruction efficiency– of  $9 \times 10^{-5}$ . Thus these two events are discarded from the  $B/S$  computation.
- One event is reconstructed from a  $\Lambda_b \rightarrow D_s p$  decay. It can be removed with a  $\Delta\mathcal{L}_{Kp}$  cut on the bachelor.



Only the latter event from the above list remains for the  $B/S$  computation. It is a specific decay which should not be downscaled by the mass ratio. Separated limits are quoted for the combinatorial background (based on zero event) and for the specific background contributions (based on one event). For the combinatorial background, the confidence interval according to [12] is:

$$\frac{B^{\text{combinatorial}}}{\bar{S}_{(B_s \rightarrow D_s^\mp K^\pm)}} \in [0, 0.18] @ 90\% \text{ CL}$$

For the specific background the  $B/S$  central value is  $0.7 \pm 0.3$  and the confidence interval is:

$$\frac{B^{\text{specific}}}{\bar{S}_{(B_s \rightarrow D_s^\mp K^\pm)}} \in [0.08, 3] @ 90\% \text{ CL}$$

However, as emphasised above, the one event comes from the  $b\bar{b}$  sample and passes the selection due to a mis-identification of a  $p$  as a  $K$ . This kind of background can be reduced to a marginal contribution with an appropriate PID cut. It has not been included here because no Monte Carlo sample of  $\Lambda_b \rightarrow D_s p$  decays was produced. Thus, the 0.18 upper limit from the combinatorial contribution is more indicative than the value of 3 quoted for the specific background.

#### 4.5 Specific B background contributions

Table 6 shows the contributions of some specific backgrounds studied with dedicated Monte Carlo samples. These contributions are computed for a tight  $B_s$  mass window ( $\pm 50$  MeV) and after the HLT trigger. The tested channels are  $B_d \rightarrow D^- \pi^+$ ,  $B_s \rightarrow D_s^- \pi^+$ ,  $B_s \rightarrow D_s^{*-} K^+$ ,  $B_s \rightarrow D_s^- \rho^+$ ,  $B_s \rightarrow D_s^- \ell^+ \nu X$  and  $B_s \rightarrow D_s^- \pi^+ \pi^- \pi^+$ . Contributions with an upper limit (90% CL) lower than  $10^{-3}$  are not reported in the table.

$B_s \rightarrow D_s^- \pi^+$ Decay channel	$B/S$	$B_s \rightarrow D_s^\mp K^\pm$ Decay channel	$B/S$
$B_d \rightarrow D^- \pi^+$	$0.044 \pm 0.014$	$B_s \rightarrow D_s^- \pi^+$	$0.15 \pm 0.05$
$B_s \rightarrow D_s^\mp K^\pm$	$0.013 \pm 0.003$	$B_s \rightarrow D_s^- \ell^+ \nu X$	$< 0.26$ at 90% CL
$B_s \rightarrow D_s^- \ell^+ \nu X$	$< 0.02$ at 90% CL	$B_s \rightarrow D_s^{*-} \pi^+$	$< 0.08$ at 90% CL
$B_s \rightarrow D_s^{*-} \pi^+$	$< 0.004$ at 90% CL	$B_s \rightarrow D_s^- \rho^+$	$< 0.06$ at 90% CL
$B_s \rightarrow D_s^- \rho^+$	$< 0.002$ at 90% CL	$B_d \rightarrow D^- \pi^+$	$< 0.03$ at 90% CL
		$B_s \rightarrow D_s^- \pi^+ \pi^- \pi^+$	$< 0.018$ at 90% CL
		$B_s \rightarrow D_s^{*-} K^+$	$< 0.006$ at 90% CL

Table 6: Specific background contributions for  $B_s \rightarrow D_s^- \pi^+$  and  $B_s \rightarrow D_s^\mp K^\pm$ .

#### 4.6 Summary

Table 7 summarises the selection results. The limits on the specific background contributions look rather high at first sight. Especially for  $B_s \rightarrow D_s^\mp K^\pm$ . However, it is important to stress that this limit is based on a single event that passes the selection. Moreover, the event that passes the  $B_s \rightarrow D_s^\mp K^\pm$  and three events out of the six specific that pass the  $B_s \rightarrow D_s^- \pi^+$  selection are  $\Lambda_b$  decays with a mis-identified proton. This shows how important it is to study the  $\Lambda_b$  decays.

	$B_s \rightarrow D_s^- \pi^+$	$B_s \rightarrow D_s^\mp K^\pm$
Total efficiency ( $\epsilon_{\text{tot}}$ )	0.39%	0.32%
Yield after trigger:	$(140 \pm 40)$ k	$(6.2 \pm 2.4)$ k
$B/S$ at 90% CL ( $b\bar{b}$ combinatorial)	$\in [0.014, 0.05]$	$\in [0, 0.18]$
$B/S$ at 90% CL ( $b\bar{b}$ specific)	$\in [0.08, 0.4]$	$\in [0.08, 3]$

Table 7: Summary of the  $B_s \rightarrow D_s^- \pi^+$  and  $B_s \rightarrow D_s^\mp K^\pm$  selection results, assuming  $2 \text{ fb}^{-1}$  of data. The errors on the yields come from the branching fraction uncertainties. The statistical errors on the yields are negligible.

The background estimates for  $B_s \rightarrow D_s^- \pi^+$  and  $B_s \rightarrow D_s^\mp K^\pm$  are computed before trigger. After the trigger, only one combinatorial is reconstructed as  $B_s \rightarrow D_s^- \pi^+$  and none as  $B_s \rightarrow D_s^\mp K^\pm$ . Thus the background 90% CL upper limits after trigger for  $B_s \rightarrow D_s^- \pi^+$  and  $B_s \rightarrow D_s^\mp K^\pm$  are 0.05 and 0.6 respectively. Because the statistics is reduced after trigger, the limit for  $B_s \rightarrow D_s^\mp K^\pm$  increases. The central value is however equal to zero.

One possible improvement could arise from the inclusion of other  $D_s$  decay modes like  $D_s^- \rightarrow \pi^- \pi^+ \pi^-$  and  $D_s^- \rightarrow K^+ \pi^- \pi^+$  which have non negligible branching fractions (1.2% and 0.7%) and almost identical signatures. This would increase the signal yield and, since the selection will be very similar, should not introduce new substantial sources of background. The increase in signal statistics could be as large as 37%, in case the selection efficiency for the additional  $D_s$  decay modes is the same as for  $D_s^- \rightarrow K^- K^+ \pi^-$ . If the background turns out to be too large when analysing real data, a solution would be to consider only resonant  $D_s^-$  decay such as  $\phi \pi^-$  and  $K^{*0} K^-$ . This leads to additional constraints in the  $D_s$  reconstruction, hence increasing the selection purity.

## 5 Properties of selected signal events

### 5.1 $B_s$ mass resolution

Figure 8 shows the reconstructed  $B_s$  mass distributions for the signal and some background sources. Histograms on each plot are normalised to  $2 \text{ fb}^{-1}$  of data. Performing a double Gaussian fit on both signal mass spectra gives  $\sigma_{B_s} = 14.0 \text{ MeV}$ .

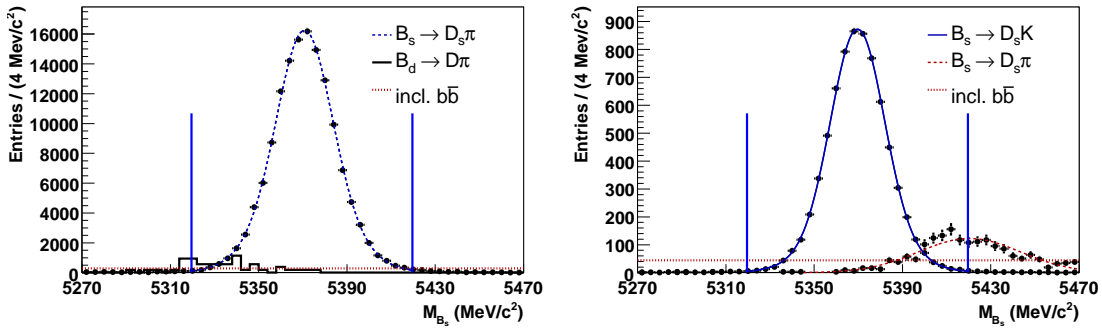
### 5.2 Proptertime reconstruction

The proptertime  $\tau$  of a  $B_s$  meson can be estimated from its reconstructed mass  $m$  and momentum  $\vec{p}$  through the relation

$$\tau = m \frac{\vec{p} \cdot \vec{FD}}{|\vec{p}|^2},$$

where  $\vec{FD}$  is the  $B_s$  meson flight distance vector (i.e. the vector between the production vertex and its decay vertex). The proptertime value and its error estimate are extracted by a dedicated algorithm<sup>10</sup>.

<sup>10</sup>`LifeTimeFitter` introduced in Ref. [13]



(a) Reconstructed  $B_s$  mass for  $B_s \rightarrow D_s^- \pi^+$  decays (b) Reconstructed  $B_s$  mass for  $B_s \rightarrow D_s^+ K^\pm$  decays

Figure 8: Reconstructed  $B_s$  mass for the signal and main backgrounds. The trigger has been applied. The upper limit of the estimated combinatorial  $b\bar{b}$  background is represented as a flat distribution (dotted line). Histograms are normalised to  $2 \text{ fb}^{-1}$  of data.

### 5.2.1 Propertime error and pull

Figure 9 shows the propertime error estimate and the propertime pull  $\frac{\tau^{\text{rec}} - \tau^{\text{true}}}{\sigma_{\tau^{\text{rec}}}}$  for  $B_s \rightarrow D_s^- \pi^+$  and  $B_s \rightarrow D_s^+ K^\pm$  together.

The estimate of the error on the reconstructed  $B_s$  lifetime has a mean value of 33 fs and a most probable value of 30 fs. The pull distribution is fitted with a Gaussian. The sigma is  $\sigma_{\text{pull}} = 1.199 \pm 0.002$ . This shows that the errors are underestimated. The mean is  $\mu = -0.075 \pm 0.002$  showing a significant bias in the propertime reconstruction. We are currently investigating on these not yet understood effects.

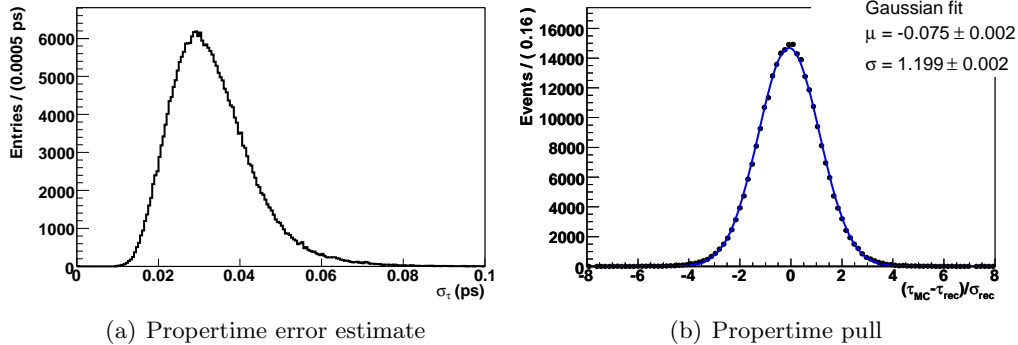


Figure 9: Error estimate and pull on the reconstructed propertime for signal events passing either the  $B_s \rightarrow D_s^- \pi^+$  or the  $B_s \rightarrow D_s^+ K^\pm$  selection (no trigger).

### 5.2.2 Selection efficiency versus reconstructed propertime

The  $B_s \rightarrow D_s h$  selection efficiency versus the reconstructed propertime is a non-flat function called here the *acceptance* function. Small propertimes are not reconstructed efficiently

due to displaced vertex requirements and the selection cuts on the impact parameter significances. Moreover, the trigger rejects also high impact parameter tracks, rejecting a fraction of the high proper time events. Figure 10 shows the acceptance function after the offline selection and the different trigger steps. The parameters of the fit are shown in the figure. The acceptance function is the ratio of two distributions, namely the reconstructed proptime after and before selection. The fitted function is

$$A(\tau) \propto \frac{(s_{\text{low}} \times \tau)^n}{1 + (s_{\text{low}} \times \tau)^n} (1 + s_{\text{high}} \times \tau),$$

where  $s_{\text{high}}$  and  $s_{\text{low}}$  are two slope parameters. The fit result shows that the inclusion of the second slope ( $s_{\text{high}}$ ) is needed, especially for events passing the trigger.

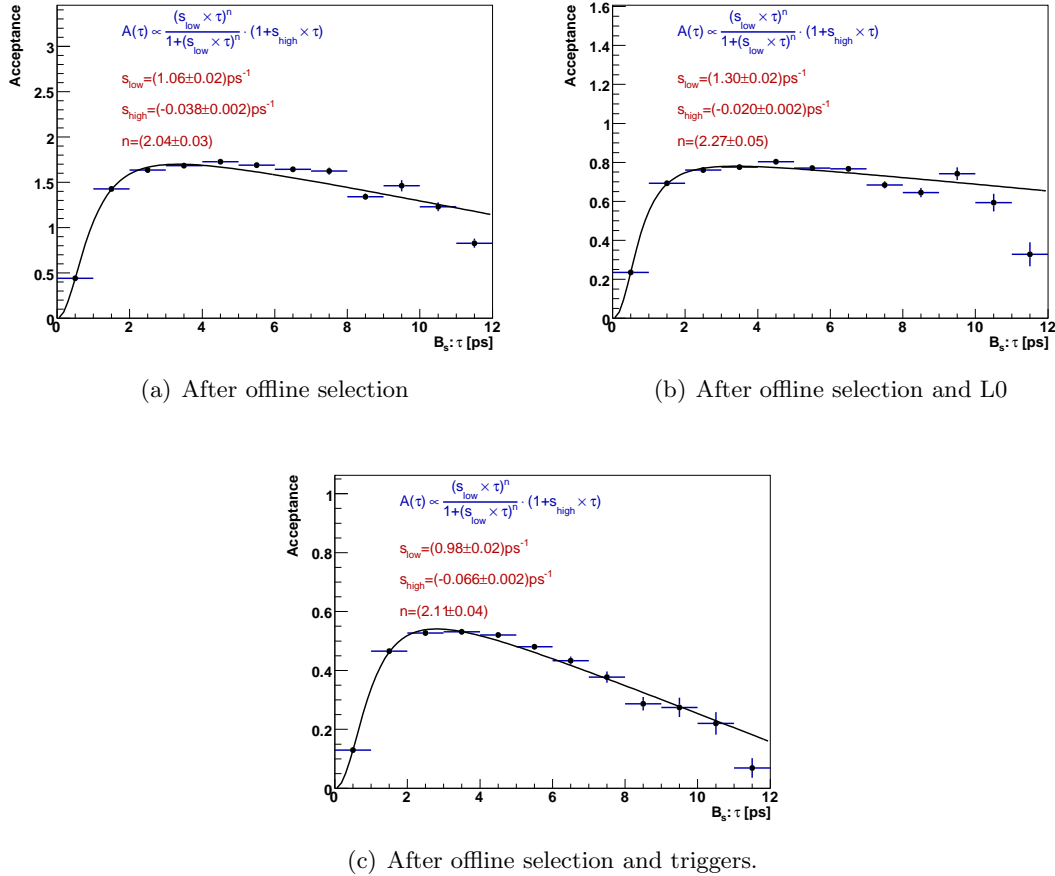


Figure 10: Reconstruction efficiency versus proptime (in ps) after the  $B_s \rightarrow D_s^- \pi^+$  offline selection and the different trigger stages.

### 5.2.3 Reconstruction of the $B_s - \bar{B}_s$ oscillation

Figure 11 shows the  $B_s$  decay rates versus the proper time at different stages of the reconstruction. The statistics correspond to  $0.5 \text{ fb}^{-1}$  of data. The  $\Delta m_s$  Monte Carlo input value is  $20 \text{ ps}^{-1}$ , while the  $\Delta \Gamma_s$  value is  $0.068 \text{ ps}^{-1}$ . The tagging<sup>11</sup> performances are shown

<sup>11</sup>Tagging software version v6r6.

in Table 8. Details about the tagging algorithms can be found in [14].

$B_s \rightarrow D_s^- \pi^+$		selected	selected and triggered
$\epsilon_{\text{tag}}$	(%)	$58.12 \pm 0.12$	$62.80 \pm 0.20$
$\omega_{\text{tag}}$	(%)	$32.80 \pm 0.15$	$30.99 \pm 0.25$
$\epsilon_{\text{eff}}$	(%)	$6.88 \pm 0.16$	$9.08 \pm 0.32$

Table 8: Tagging efficiencies, wrong tag fractions and total efficiencies for selected events before and after the triggers.

The plots in Fig. 11 are obtained from reconstructed  $B_s \rightarrow D_s^- \pi^+$  signal events with no background. The  $B_s$  flavour comes either from Monte Carlo information (Fig. 11(a), 11(b) and 11(c)) or from the tagging algorithm (Fig. 11(d), 11(e) and 11(f)). The flavour at decay is deduced from the reconstructed bachelor charge. The shaded histograms represent the events which have mixed (initial  $B_s$  decaying to an  $D_s^+ \pi^-$  state or initial  $\bar{B}_s$  decaying to  $D_s^- \pi^+$ ). The other histograms represents all events.

Figure 11(a) shows the distribution of the proptime for the Monte Carlo events. Figure 11(b) is also based on the Monte Carlo information, but only for signal events that passed the  $B_s \rightarrow D_s^- \pi^+$  selection. Figure 11(c) shows the reconstructed proptime for the selected events. The tagging information however is still taken from the Monte Carlo. Figure 11(d) shows the true proptime for selected and tagged events where the tagging algorithm has been applied. It also shows the distribution for all the events (tagged and untagged). Thus some wrong tag is present, reducing the oscillation amplitude. Figure 11(e) shows the reconstructed proptime with the tagging algorithm applied. Figure 11(f) is the same as Figure 11(e) but the selected events also pass the triggers. Hence this plot, although without background, shows what will be reconstructed with the real data.

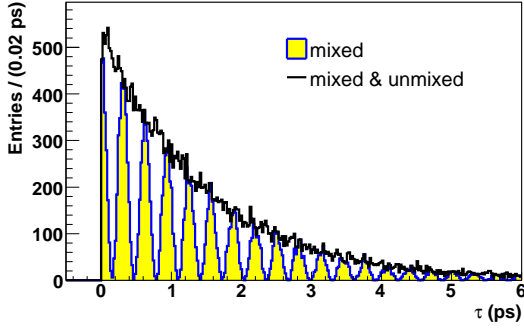
Comparing the plots in Fig. 11(c) with Fig. 11(d), we see that the effect of the proptime resolution is similar (although with a different scale) to the effect of the wrong-tag fraction: both reduce the amplitude of the oscillation. Due to this correlation, their simultaneous extraction will be difficult. It is therefore foreseen to extract the proptime resolution from another data sample, such as prompt  $J/\psi$ .

## 6 Sensitivity to $\Delta m_s$

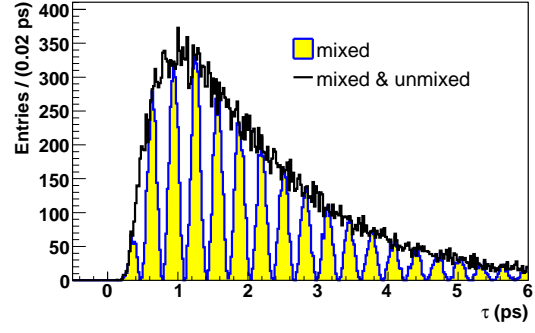
A fast Monte Carlo study [15, 16] based on the results presented in this document has been performed. It uses a  $B/S$  ratio of 0.4 for the  $B_s \rightarrow D_s^- \pi^+$  selection, a wrong tag fraction  $\omega_{\text{tag}}$  of 31% and a tagging efficiency of  $\epsilon_{\text{tag}}$  of 63% which are the values for triggered and selected events. The  $\Delta m_s$  value is  $17.5 \text{ ps}^{-1}$ , the  $B_s$  mean decay time is  $\tau_s = 1/\Gamma_s = 1.45 \text{ ps}$  and  $\Delta\Gamma_s/\Gamma_s = 0.15$ . The per-event error estimate distribution is shown in Figure 9(a). The annual yield of  $B_s \rightarrow D_s^- \pi^+$  events is<sup>12</sup> 140 k. It allows to determine the LHCb sensitivity to the  $\Delta m_s$  and the  $\omega_{\text{tag}}$  parameters with  $2 \text{ fb}^{-1}$  of data:

$$\begin{aligned} \sigma(\Delta m_s) &= \pm 0.006, \text{ for } \Delta m_s = 17.5 \text{ ps}^{-1} \\ \sigma(\omega_{\text{tag}}) &= \pm 0.0033, \text{ i.e. } \sigma(\omega_{\text{tag}})/\omega_{\text{tag}} = 0.011. \end{aligned}$$

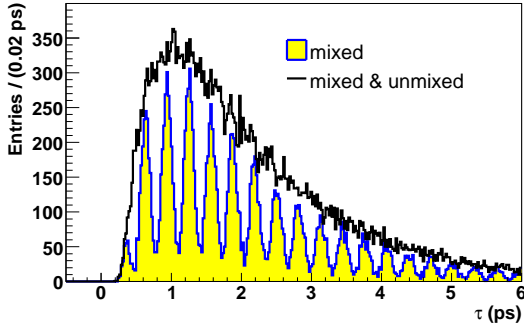
<sup>12</sup>The study, originally done with a yield of 120 k, has been scaled here to the value of 140 k because the  $B_s \rightarrow D_s^- \pi^+$  branching ratio has changed in the mean time.



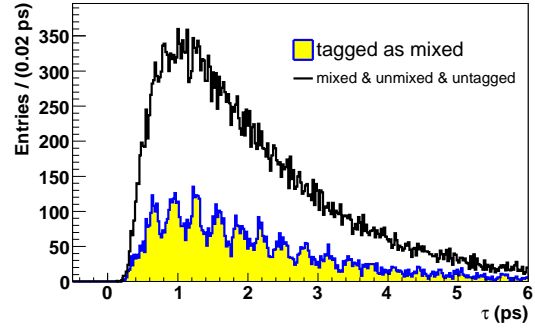
(a) True proper time distribution



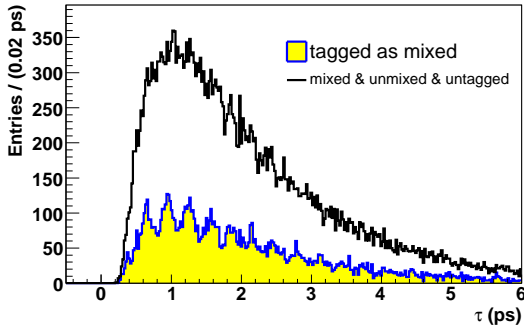
(b) True proper time distribution for selected events



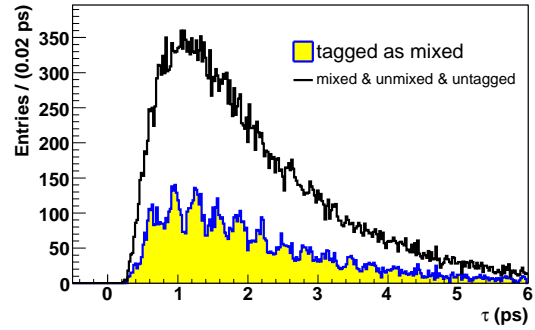
(c) Reconstructed proper time distribution for selected events, tagging based on the Monte Carlo



(d) True proper time distribution for selected and tagged events



(e) Reconstructed proper time distribution for selected and tagged events



(f) Reconstructed proper time distribution for selected tagged and triggered events

Figure 11: Proper time distributions of  $B_s \rightarrow D_s^- \pi^+$  signal events corresponding to  $0.5 \text{ fb}^{-1}$  of data at different stages of the full simulation and reconstruction.

## 7 Conclusion

This study based on DC04 Monte Carlo data shows the results of the  $B_s \rightarrow D_s h$  offline selection. The number of selected and triggered  $B_s \rightarrow D_s^- \pi^+$  and  $B_s \rightarrow D_s^\mp K^\pm$  events per  $2 \text{ fb}^{-1}$  is  $140 \text{ k} \pm 40 \text{ k}$  and  $6.2 \text{ k} \pm 2.4 \text{ k}$  respectively. The uncertainties come from the branching fractions and the  $B_s$  production fraction and do not include the error on the  $b\bar{b}$  cross section.

The present study gives  $B/S$  upper limits for the combinatorial background: 0.05 and 0.18 for  $B_s \rightarrow D_s^- \pi^+$  and  $B_s \rightarrow D_s^\mp K^\pm$  respectively. The  $b\bar{b}$  specific background contribution upper limits are 0.4 and 3. Separated studies have been done on  $B_d \rightarrow D^- \pi^+$ ,  $B_s \rightarrow D_s^{*-} \pi^+$ ,  $B_s \rightarrow D_s^{*-} K^+$ ,  $B_s \rightarrow D_s^- \ell^+ \nu X$ ,  $B_s \rightarrow D_s^- \rho^+$  samples to quantify these particular backgrounds. The results show that the main contribution to  $B_s \rightarrow D_s^- \pi^+$  comes from  $B_d \rightarrow D^- \pi^+$ , with a  $B/S$  of  $0.044 \pm 0.014$ . For  $B_s \rightarrow D_s^\mp K^\pm$  the main contribution to the background is  $B_s \rightarrow D_s^- \pi^+$ , with a  $B/S$  of  $0.15 \pm 0.05$ .

## References

- [1] LHCb Collaboration, S. Amato et al. “LHCb Reoptimized Detector Design and Performance”. CERN/LHCC 2003-030, 2003.
- [2] G. Branco et al. “CP Violation”. Oxford University Press, New York, 1999.
- [3] LHCb EvtGen web site. <http://lhcb-release-area.web.cern.ch/LHCb-release-area/DOC/gauss/generator/evtgen.php>.
- [4] L. Nicolas. “Selection and study of the  $B_s^0 \rightarrow D_s^- \pi^+$  decay at LHCb”. LPHE, EPFL Master thesis, 2005.
- [5] W.-M. Yao et al. (Particle Data Group). Review of Particle Physics. *Journal of Physics G*, 33:1+, 2006.
- [6] S. Stone. “Hadronic Charm Decays and D Mixing”. hep-ph/0605134, 2006.
- [7] CDF Collaboration, A. Abulencia et al. “Measurement of the Ratios of Branching Fractions  $B(B_s^0 \rightarrow D_s^- \pi^+ \pi^+ \pi^-)/B(B_d^0 \rightarrow D^- \pi^+ \pi^+ \pi^-)$  and  $B(B_s^0 \rightarrow D_s^- \pi^+)/B(B_d^0 \rightarrow D^- \pi^+)$ ”. hep-ex/0610045, 2006.
- [8] Belle Collaboration, K. Abe et al. “Measurements of exclusive  $B_s^0$  decays at the  $\Upsilon(5S)$ ”. BELLE-CONF-0615, 2006.
- [9] ALEPH Collaboration, D. Buskulic et al. “Measurement of the  $B_s^0$  lifetime and production rate with  $D_s^-$  lepton $^+$  combinations in Z decays”. Phys. Lett. B361:221-233, 1995.
- [10] OPAL Collaboration, P.D. Acton et al. “Evidence for the existence of the strange b flavored meson  $B_s^0$  in  $Z^0$  decays”. Phys. Lett. B295:357-370, 1992.
- [11] DELPHI Collaboration, P. Abreu et al. “Evidence for  $B_s^0$  meson production in  $Z^0$  decays”. Phys. Lett. B289:199-210, 1992.
- [12] Feldman et al. “Unified approach to the classical statistical analysis of small signals”. PhysRevD.57.3873, 1998.
- [13] G. Raven. “Selection of  $B_s \rightarrow J/\psi \phi$  and  $B^+ \rightarrow J/\psi K^+$ ”. CERN-LHCb-2003-118, 2003.

- [14] M. Calvi and others. “Flavour Tagging algorithms and performance in LHCb”. LHCb-2007-058, 2007.
- [15] L. Fernández. “Sensitivity to the  $B_s - \bar{B}_s$  Mixing Phase at LHCb”. LHCb-2006-047, 2006.
- [16] L. Fernández. “Exclusive trigger selections and sensitivity to the  $B_s - \bar{B}_s$  mixing phase at LHCb”. EPFL thesis 3613, CERN thesis 2006-042, 2006.